Paper to be Submitted for Presentation in ECS2005
The European Coating Symposium 2005

A Novel Predictive Model for Tri-Helical Gravure Roll Coating

R W Hewson, N Kapur *and* ***P H Gaskell***

School of Mechanical Engineering, University of Leeds, Leeds. LS2 9JT. UK.

Abstract

Tri-helical, gravure roll coating, operating in reverse mode, is investigated both experimentally and theoretically for grooves of different cross section and helix angle orientation. The flow is modelled using lubrication theory and the resulting hydrodynamic pressure equation solved using finite elements. It is shown that a stable operating window exists such that as the web to gravure roll speed ratio increases then so to does the fraction of fluid transferred onto the web; increased helix angle having the effect of decreasing the amount of fluid transferred at the same speed ratio. The agreement between the theoretical predictions and experimental data are found to be good for helix angles up to and including 45°, with the assumptions underpinning the model being questionable beyond this point and requiring further refinement.

1 Introduction

Gravure roll coating is a process used widely within industry to deposit thin liquid films of 1 to $50\mu m$ depth onto a range of moving flexible substrates. The tri-helical subset of available gravure rolls have a series of continuous spirals engraved or knurled into their surface. The mode of operations is simple, a semi-submerged gravure roll entrains fluid from a coating bath onto its surface; excess fluid is doctored from it leaving fluid within the spiral grooves. The substrate (web) then passes over the roll where fluid transfer occurs. The process can be operated in either forward or reverse mode, with the web and roll passing though the coating bead in the same or opposite direction, respectively. The reverse mode is the more commonly encountered form of tri-helical gravure roll coating due to its larger stable operating window [1], which is similarly observed in fixed gap twin roll coating [2]. A cross sectional schematic of the process is shown in figure 1.

The present work models the above process as an inertialess flow, the governing equations taking the form of a two dimensional Poisson's equation in the groove direction and a one dimensional Poisson's equation for the cross-directional flow. Simple meniscus models make the associated hydrodynamic pressure equations tractable. The predictions obtained are compared against a comprehensive set of complementary experimental data collected as part of the same investigation.

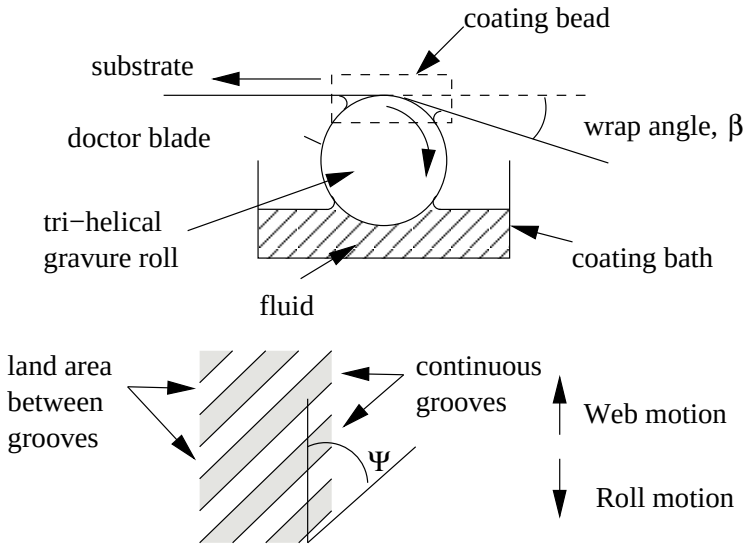

Figure 1: Cross sectional schematic of a reverse gravure roll coating arrangement, together with an illustration of the angled, Ψ, groove arrangement present on the surface of the tri-helically patterned roll.

2 Experimental Setup

A schematic outline of the coating rig used to perform the experiments and collect the necessary data is shown in figure 2. The apparatus utilises gravure rolls of length 200mm and diameter 100mm having a maximum peripheral speed of $U_{Roll} = 100m/s$; included also are controls for web tension, velocity and wrap angle. The rolls are comprised of an acrylic sleeve mounted with grub screws on a central steel core. Film thickness measurements were made by scraping fluid from the web over a measured time. The residual fluid remaining on the lands after scraping was found to be negligible. The fluids used in the experiments were Newtonian water-glycerol mixtures with a small volume of surfactant to reduce surface tension and improve wetting. Viscosity covered the range of $\mu = 0.002$ to $0.0075Pas$, with surface tension $\sigma = 0.033$ to $0.065N/m$. A set of 12 rolls was manufactured with cross sectional groove dimensions as defined in figure 3 and listed in table 1 (note, groove dimensions are taken as perpendicular to groove direction, not along the direction of the roll axis).

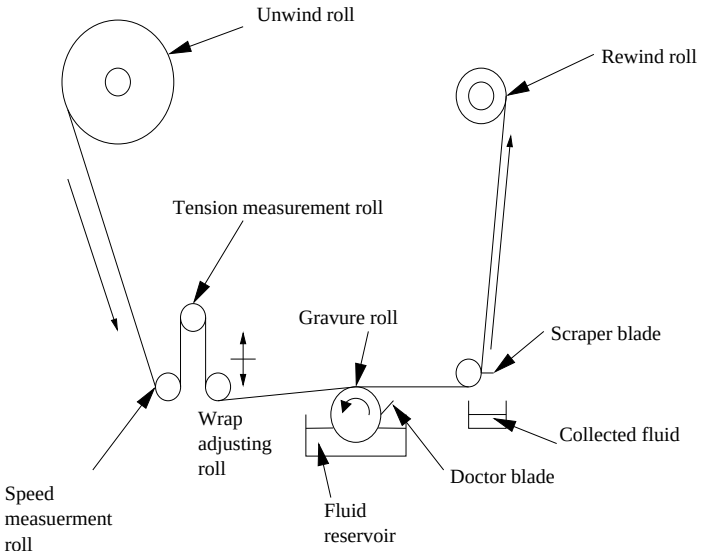

Figure 2: Cross sectional outline of the experimental coating apparatus.

Figure 3: Characteristic groove dimensions; groove width *A*, land width *B* and groove depth *C*.

Roll	Groove Type	Groove Width *A* (mm)	Land Width *B* (mm)	Groove Depth *C* (mm)	Groove Angle Ψ
A1	Rectangular	0.47	0.53	0.18	0°
A2	Rectangular	0.47	0.54	0.35	0°
A3	Rectangular	0.47	0.53	0.30	0°
B1	Triangular	0.71	0.29	0.52	0°
B2	Triangular	0.82	0.18	0.60	0°
B3	Triangular	0.80	0.20	0.39	0°
C1	Rectangular	0.50	0.50	0.4	30°
C2	Rectangular	0.50	0.50	0.4	45°
C3	Rectangular	0.40	0.60	0.4	60°
D1	Triangular	0.33	0.25	0.30	30°
D2	Triangular	0.30	0.14	0.30	45°
D3	Triangular	0.30	0.29	0.30	60°

Table 1: Rectangular and triangular, radially cut, groove data (see figure 3 for groove dimensions).

3 Mathematical Model

The mathematical model described below enables the pressure distribution throughout the coating bead to be found by means of an iterative approach; a search is made to obtain the flux through the coating bead for which the pressures imposed at the bounding free surfaces via simple meniscus models and the pressure gradients in the coating bead are consistent. There are therefore two components to the model, the governing hydrodynamic equations for the pressure distribution generated in the coating bead driven by the relative motion of the web and roll surfaces, and the bounding upstream and downstream meniscus conditions (with reference to where the web enters and leaves the coating bead respectively).

3.1 Hydrodynamic Equations

As the grooves are angled with respect to the direction of web motion the problem is divided into the flow in the groove direction and that in the cross flow direction (as shown in figure 4). Scaling parameters are given in appendix A.

3.1.1 x'-direction flux

By neglecting inertial forces the Navier-Stokes equations simply result in a two dimensional Poisson's equation,

$$\frac{dp}{dx} = \frac{d^2u}{dy^2} + \frac{d^2u}{dz^2}, \tag{1}$$

an assumption consistent with that used to obtain the lubrication equations. The x'-direction flux is obtained by integrating equation (1) numerically subject to the boundary conditions that the web is moving with velocity $S\cos\Psi$ and the groove walls with velocity $\cos\Psi$. A Bubnov-Galerkin weighted residuals finite element method is used with linear triangular elements to discritise the solution domain and solve the unknown, u, in equation (1) by applying the divergence theorem [3]. Recognising and imposing symmetry conditions along groove and land centres minimises the size of solution domain, with approximately 100 nodes required to produce grid independent solutions.

3.1.2 y'-direction flux

Determining y'-direction flux is achieved by simplifying the problem, enabling an analytical solution to be found. The assumptions made are:

a) that the flux contained within the grooves is transported by the roll with velocity $\sin\Psi$;

b) that in the web-roll gap the flux is determined by Poiseuille-Couette flow;

a consequence of the groove angle increasing towards 90° is that the flux coated on the web becomes zero since a rigid web model is adopted.

The flux due to a) is determined from the velocity of the roll in the y'-direction, the equivalent film thickness (the average depth of fluid on the roll) and the distance the flux passes though per groove ($(1+b)\tan\Psi$). The contribution to the flux from a) is therefore:

$$Flux = \underbrace{k}_{\text{average groove depth}} \times \underbrace{(1+b)\tan\Psi}_{\text{groove dimension projected in the } y' \text{ direction}} \times \underbrace{\sin\Psi}_{\text{roll velocity}} . \tag{2}$$

The component of flow due to b) is determined by assuming Couette-Poiseuille flow, based

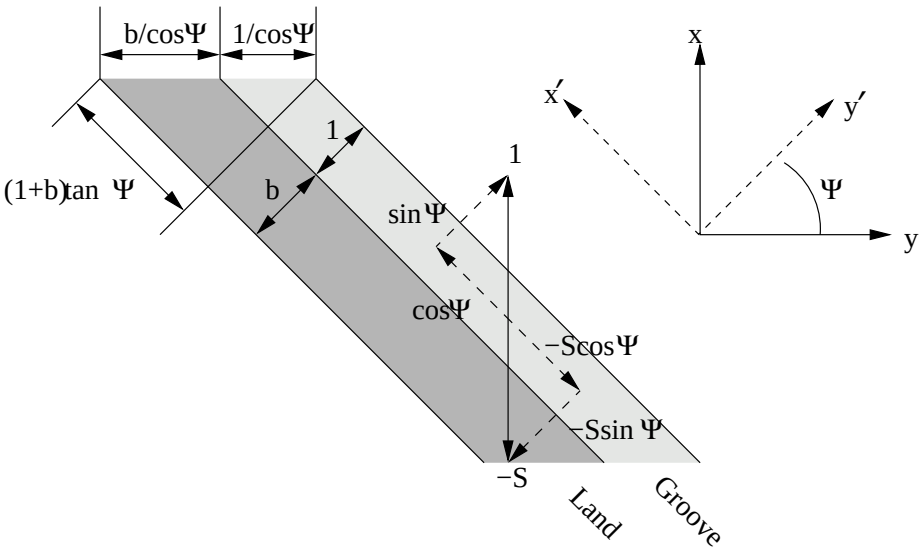

Figure 4: Resolution of velocities in coating model: groove component, $S\cos\Psi$; cross groove component, $S\sin\Psi$.

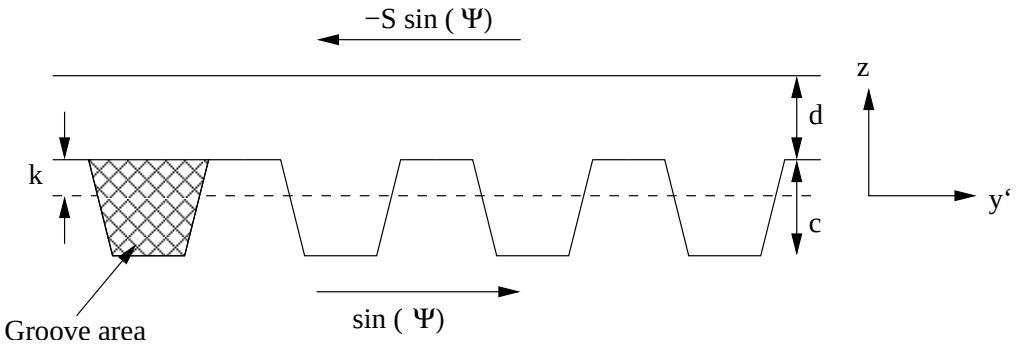

Figure 5: Cross Flow Geometry

on the following equation,

$$\frac{d^2v'}{dz^2} = \frac{dp}{dy'} \equiv \frac{dp}{dx}\sin\Psi. \tag{3}$$

Integrating equation (3) twice with respect to z gives,

$$v' = \frac{z^2}{2}\frac{dp}{dx}\sin\Psi + zc_1 + c_2. \tag{4}$$

Due to the varying geometry in the y'-direction an average groove depth is used and the boundary conditions required to solve (4), based on the roll and web's peripheral speeds, are,

$$v' = \sin\Psi \quad \text{at} \quad z = 0 \quad \text{and} \quad v' = S\sin\Psi \quad \text{at} \quad z = d + k. \tag{5}$$

Application of these boundary conditions results in an equation that describes the "averaged" velocity distribution, which is integrated from the roll land to the web. This effectively provides a level of slip at the roll surface to account for the intermittency of the roll surface. The final flux per groove in the y'-direction is therefore,

$$\begin{aligned} q_{y'} = & \frac{\sin(\Psi)\,d\,(d+2k)\,(1+b)\tan(\Psi)}{2d+2k}S \\ & - \frac{\sin(\Psi)\,d^2\,(d+3k)\,(d+k)\,(1+b)\tan(\Psi)}{12d+12k}\frac{dp}{dx} \\ & + \frac{\sin(\Psi)\,(1+b)\tan(\Psi)\left(d^2+2dk+2k^2\right)}{2d+2k}. \end{aligned} \tag{6}$$

3.1.3 Pressure Gradient Solution

The overall flux per groove, obtained by adding the flux per groove in the x'- and y'-directions, is used to obtain the pressure distribution though the coating bead, the linear relationship between pressure gradient and flux making the determination of the former straightforward.

3.2 Bounding Meniscus Conditions

A means of describing the locations of and pressure discontinuities across the upstream and downstream menisci is required in order to close the problem. The meniscus models employed are based on the Coyne & Elrod film forming one [4].

The downstream meniscus is assumed to be two dimensional as the grooves enter the coating pool full of fluid; visual inspections when carrying out experiments were made to ensure that the downstream meniscus generally remained two dimensional in nature with minimal variation in meniscus geometry in the y-direction (aligned along the groove axis).

The model used to determine the upstream meniscus pressure and location is based on the idealised case of rectangular grooves aligned with the direction of the flow, i.e. $\Psi = 0$ [5, 6]. By relating the generalised groove geometry to that of rectangular grooves the residual liquid films on the walls of the roll were calculated based on the distances between surfaces. The dynamic contact angle was catered for using the empirical model of Jiang, Oh and Slattery [7].

3.3 Calculation Procedure

The method used to determine the flux is the same as that used by Hewson et al. [6]. A search for the flux which results in consistent pressures throughout the coating bead is made. The resulting flux is the one for which the pressure at the downstream meniscus based on, i) the downstream meniscus model and ii) the upstream meniscus and the numerical integration of the pressure gradients, are the same.

4 Results

Fluid pickout, Φ, results, for three different grooves angles, are given in figures 6, 7 and 8. Clear agreement between experiment and theory can be observed with groove angles of 30° and 45° for speed ratios less than 1.2 and 2, respectively. Within these ranges the variation of pickout with speed ratio is approximately linear with a slight divergence from linearity with increasing groove angle, observed both experimentally and theoretically. The agreement worsens at speed ratios beyond these values, due to streaking on the web caused by the upstream meniscus passing along the grooves to the downstream side, a region which is outside the validity of the assumptions underpinning the model. As speed ratio increases towards that at which streaking first occurs the upstream meniscus is observed to move towards the point where the web and roll first come into contact- it is when the upstream meniscus and this point coincide that streaking first appears on the web, in that the bead is now bounded upstream by a series of discrete menisci, each sitting within their own groove and periodically accelerating downstream, resulting in the streaking defect.

The effect of groove angle on pickout is seen in figure 9; pickout decreases as the groove angle increases, the decrease leading to a delay in the onset of streaking for a given speed ratio. The 60° angle groove results display some interesting features. The first is that agreement is best for low speed ratios, but beyond $|S| > 1$ there is a clear divergence between theory and experiments. This can be explained as a break down in the model in that as the groove angle increases the process becomes more like a two dimensional discrete cell problem. The model is unable to predict the pickout from this configuration as it assumes a non-deformable web is present, and for which discrete cell gravure roll coating would predict a zero flux.

Figure 10 shows the pressure distribution through the coating bead, an interesting result of which is the magnitude and sign of the pressures throughout the bead as the groove angle increases. For low groove angles the predicted pressures are entirely sub-ambient and it would therefore be expected that were the web able to deform it would do so towards the roll and into the narrow grooves; the magnitude of the pressure and the narrow groove widths minimising the effect. However, for large groove angles there is a large positive pressure within the coating bead, which practically would deform the web away from the roll and produce a web to roll gap even when a non-deformable web model predicts that the web is in contact with the roll. The magnitude of the pressures throughout the coating bead increase as the speed ratio increases, thus increasing deformation of the web. This is an explanation as to why there is divergence in agreement between theory and experiments fo $S \approx 1$.

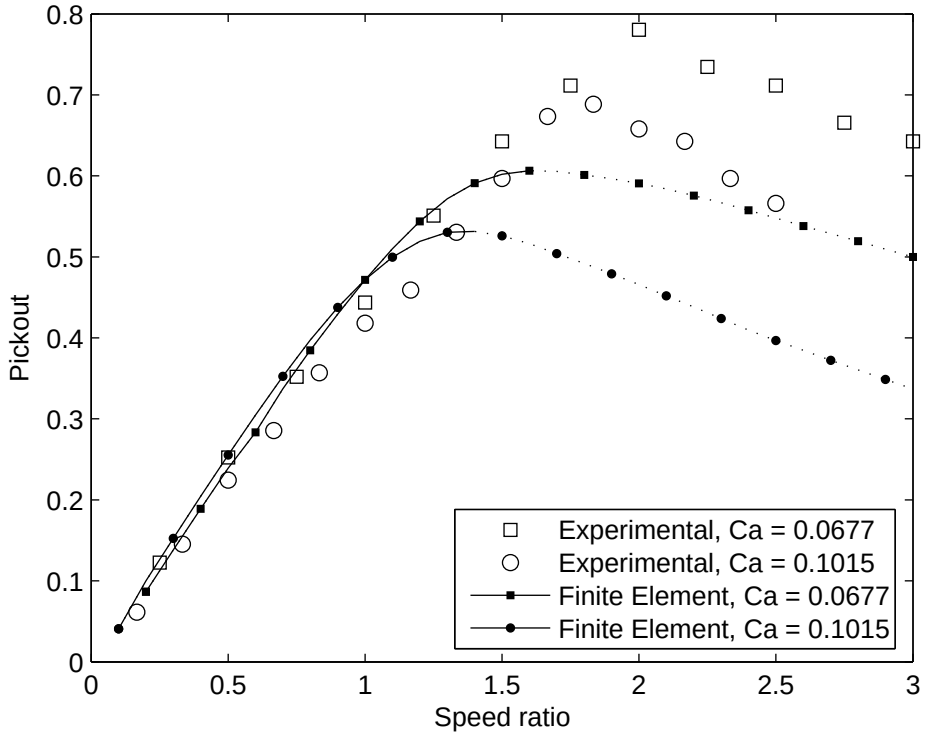

Figure 6: Roll D1, $\beta = 0^\circ$, $\Psi = 30^\circ$

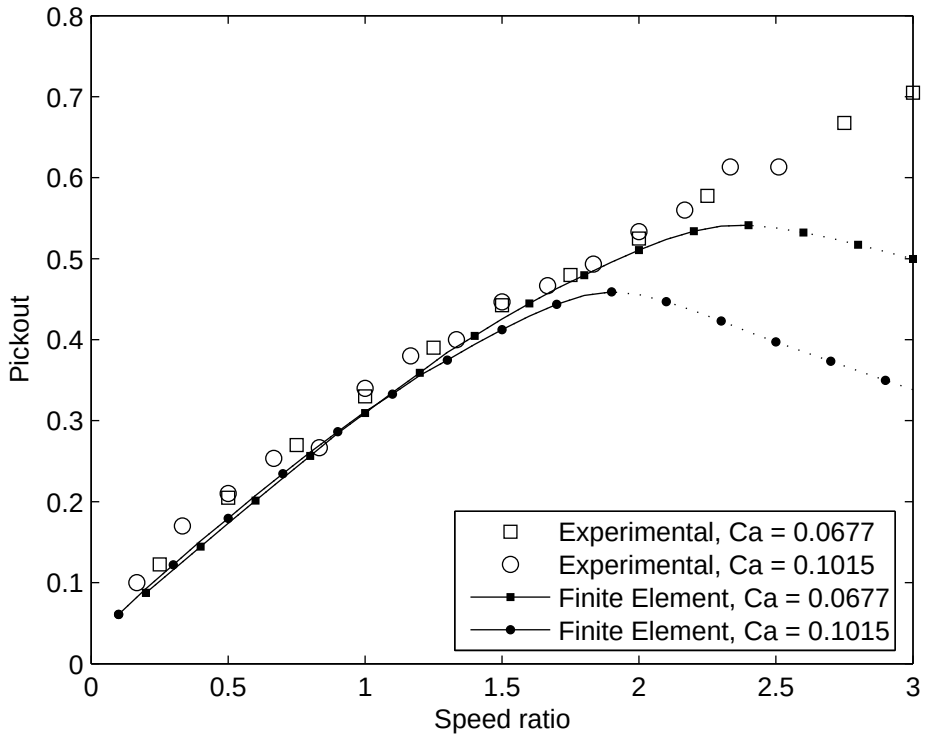

Figure 7: Roll C2, $\beta = 5^\circ$, $\Psi = 45^\circ$

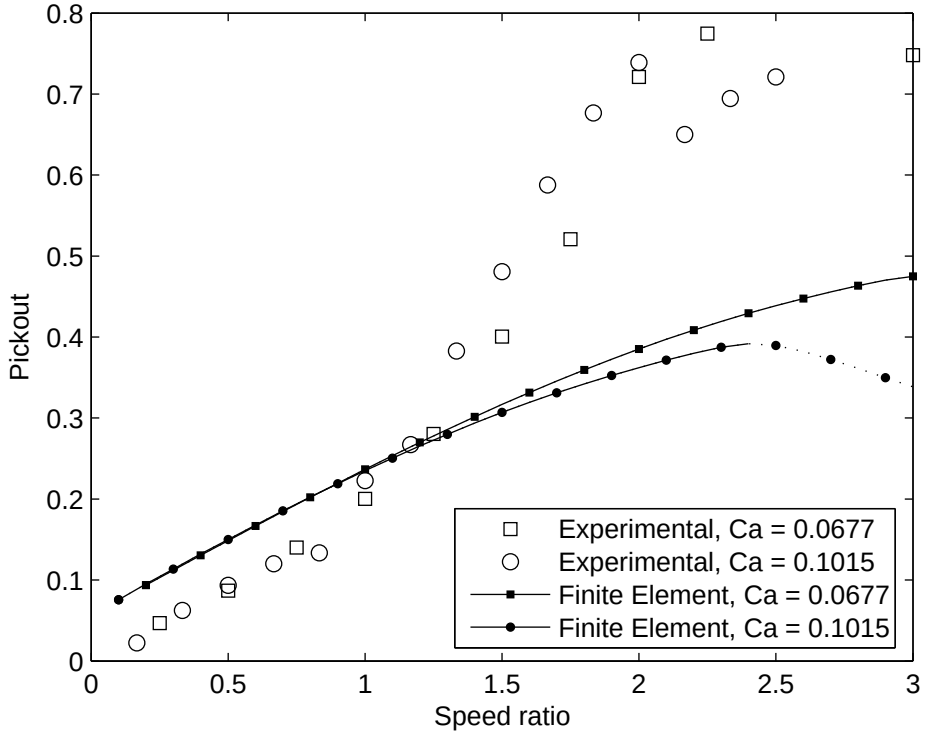

Figure 8: Roll D3, $\beta = 5°$, $\Psi = 60°$

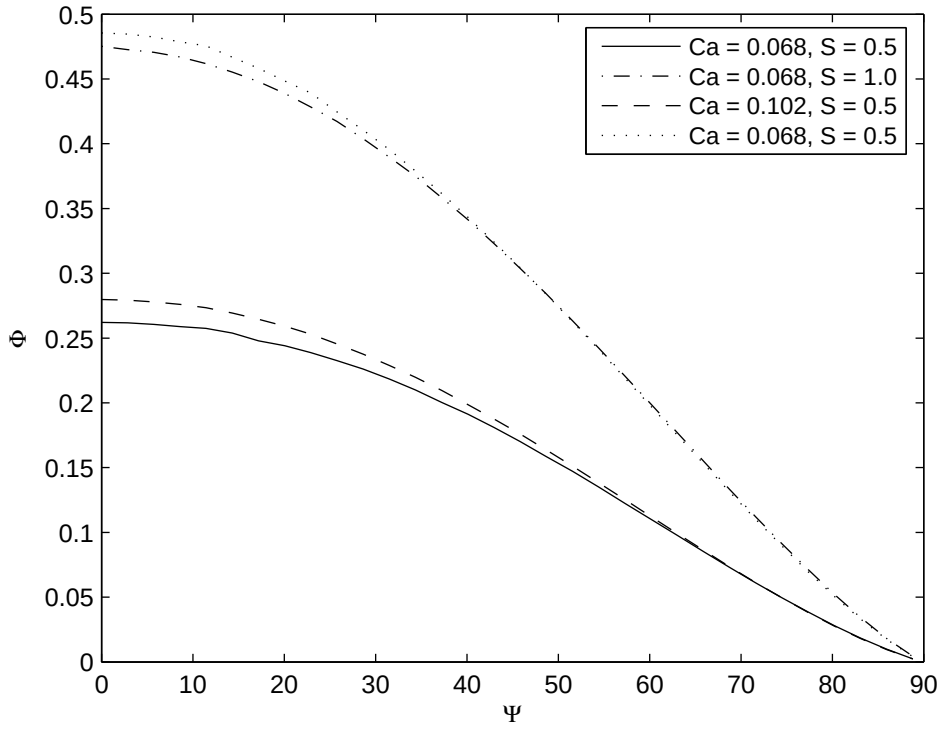

Figure 9: Rectangular groove angle results for grooves, $\beta = 5°$, $b = 1$, $c = 1$ and $r_{roll} = 100$.

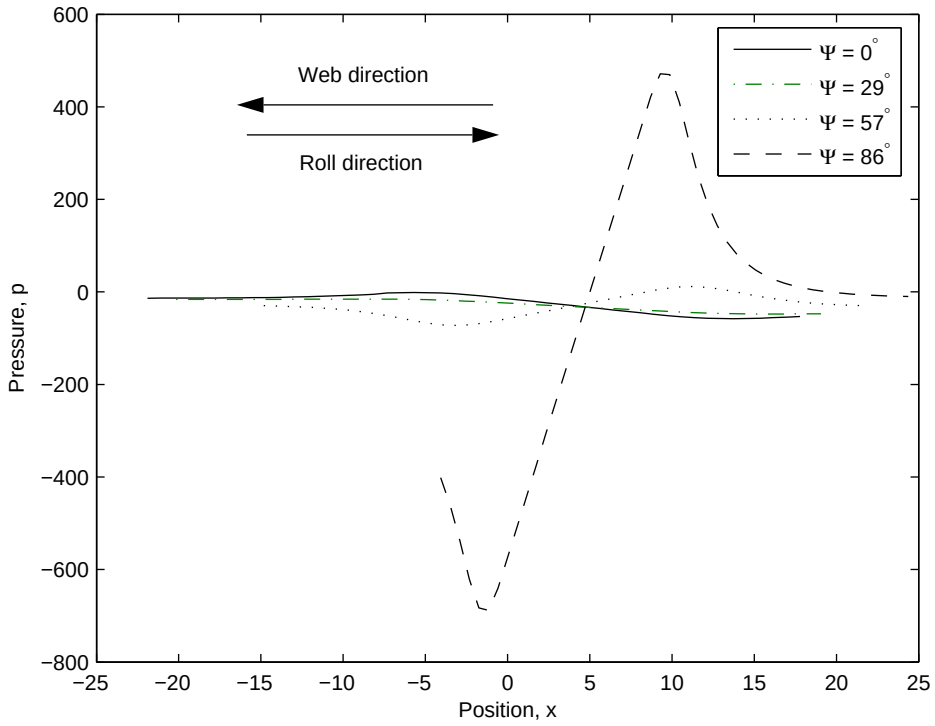

Figure 10: Rectangular groove angle results, $Ca = 0.068$, $\beta = 5°$, $b = 0.8$, $c = 1$ and $r_{roll} = 100$.

5 Conclusion

A model is presented which is shown to reliably predict the pickout and therefore film thickness for a variety of tri-helical gravure groove geometries and groove angles. Groove angle is found to decrease pickout and therefore film thickness for a given speed ratio. As the groove angle increases the onset of streaking is delayed due to lower pickout, allowing the coating process to operate at greater speed ratios. The model breaks down at higher groove angles, especially for higher speed ratios. This is due to increasing positive pressures generated within the coating bead which in practice would lead to deformation of the web but which is unaccounted for in the present model.

Acknowledgments

This work is funded by the Engineering and Physical Sciences Research Council UK (EPSRC Grant Reference: GR/R70064/01) with additional support from Dupont Teijin Films UK Ltd.

A Dimensionless Scalings

The following non-dimensional scalings are used throughout the analysis.

$$[x,y,z,1,l,d,r,k,r_{roll}] = \frac{[X,Y,Z,a,L,D,R,K,R_{roll}]}{A}, \quad S = \frac{U_{web}}{U_{roll}}, \quad p = \frac{PA}{\mu U_{roll}}, \quad Ca = \frac{\mu U_{roll}}{\sigma}$$

References

[1] H. Benkreira and O. Cohu. Direct forward gravure coating on unsupported web. *Chemical Engineering Science*, 53(6):1223–1231, 1998.

[2] D. J. Coyle. Knife and roll coating. In S. F. Kistler and P. M. Schweizer, editors, *Liquid Film Coating*, pages 539–571. Chapman and Hall, first edition, 1997.

[3] J. L. Summers. The finite element method for fluid flow problems. In *Series of lecture given by the EFM research group*, Leeds, 2003. University of Leeds.

[4] J.C. Coyne and H.G. Elrod. Conditions for the rupture of a lubricating film. part 1: Theoretical model. *Journal of Lubrication Technology*, 92:451, 1970.

[5] R. W. Hewson, N. Kapur, and P. H. Gaskell. Modelling and analysis of tri-helical gravure roll coating. In *International Coating Science and Technology Symposium*, Rochester, NY., 2004.

[6] R.W. Hewson, N Kapur, and Gaskell P. H. A theoretical and experimental investigation of tri-helical gravure roll coating. *Submitted to Chemical Engineering Science*, 2005.

[7] K.M. Jiang, S. Oh, and J.C. Slattery. Correlation for dynamic contact angle. *Journal of Colloid and Interface Science*, 69(1):74–77, 1979.